MINIATURIZED MULTILAYER DUAL-MODE SUBSTRATE INTEGRATED WAVEGUIDE FILTER WITH MULTIPLE TRANSMISSION ZEROS

Ziqiang Xu[1, *] and Hong Xia[2]

[1]Research Institute of Electronic Science and Technology, University of Electronic Science and Technology of China, Chengdu 611731, China

[2]School of Mathematical Sciences, University of Electronic Science and Technology of China, Chengdu 611731, China

Abstract—A compact multilayer substrate integrated waveguide (SIW) dual-mode filter with multiple transmission zeros for high-selectivity application is presented. By introducing mixed coupling between source and load, the proposed filter could have four transmission zeros which can be controlled flexibly. Owing to the multilayer structure, the proposed filter occupies similar area in comparison with conventional dual-cavity dual mode SIW filters, but exhibits better frequency selectivity. An experimental filter with a center frequency of 10 GHz is designed using low temperature co-fired ceramic (LTCC) technology to validate the proposed structure, and measured results agree well with simulated ones.

1. INTRODUCTION

Bandpass filters with high integration and sharp skirts are essential in the development of modern wireless and mobile communication systems [1–6]. Microwave dual-mode filters with microstrip or metal waveguide structure can provide valid solutions to satisfy these requirements owing to their high performance and easy design [7] Although the microstrip dual-mode filters are have been widely used and implemented, they have lower power-handing capability and lower resonator Q factor in higher frequencies [8, 9]. Besides, the metal waveguide dual mode filters have excellent performance owing to their high Q factor and power-handling capability. However, they cannot be easily integrated with planar microwave circuits. Meanwhile, a

high precision mechanical adjustment or a subtle tuning mechanism is needed to obtain satisfying filters [10–12]. Recently, the substrate integrated waveguide (SIW) which is synthesized in a planar substrate with arrays of metallic via, can provided an effective method to design low-cost, low-profile, and easy-integration waveguide dual-mode filters while maintain high performance as conventional metal waveguide filters [13–15]. SIW dual mode filters can be fabricated by using the printed circuit board (PCB) or low temperature co-fired ceramic (LTCC) processes [16–20]. Particularly, the application of LTCC technology makes the implement of dual-mode SIW filters with compact size, light weight and easy integration possible, due to its low loss of high-frequency ceramic materials, three dimensional integration features, and low-tolerance in manufacturing process [21, 22].

On the other hand, in order to meet the increasing demands of modern communication systems in regards to high frequency selectivity, filters are required to design with multiple transmission zeros without enlarging occupying sizes of the filter. A SIW dual-mode cavity can support two degenerate modes within one resonant unit, which not only reduces the circuit size more than half but also enhances the design flexibility [23, 24]. Ordinarily, a conventional single-cavity dual mode filter can obtained no more than one transmission zero. In order to generate more transmission zeros in finite frequency, many approaches have been implemented to design dual mode SIW filters. In [25], a dual-mode SIW filter has been designed by introducing slot lines perturbation, and two transmission zeros are allocated at each side of its passband. A single-cavity dual-mode filter in [26] which used a coplanar waveguide as a non-resonating node (NRN) to obtain indirect cross-coupling is proposed, and there are two transmission zeros located at 4.6 and 5.45 GHz. In our previous work [27], by introducing mixed coupling between source and load, the proposed filter could have three transmission zeros which can be controlled flexibly. Besides, cascading two adjacent dual-mode cavities is yet another approach to generate more transmission zeros. In [28], a SIW filter with two adjacent dual-mode resonators is designed to generate up to two transmission zeros. Although the proposed filters in [25–28] can obtain two or three transmission zeros, they are still implemented in planar and single layer structure. More recently, the multilayer technology has become important, and is also another efficient process to achieve compact circuits. Accordingly, the dual-mode and multilayer techniques can be employed together to achieve more compact SIW circuits. In [29, 30], by stacking dual-mode cavities vertically, two 3-D quasi-elliptic SIW filters with two transmission zeros in the stopband are implemented using LTCC

technology respectively. In [31], a Ka-band LTCC 4-pole bandpass filter is proposed using multilayer dual-mode circular SIW cavities, and the filter can have quasi-elliptic frequency response and two transmission zeros located at each side of the passband. Similarly, by constructing vertically with two circular cavities, a dual mode filter with two transmission zeros at upper side of the passband is presented in [32] The above described filters with compact-integration structures have good performances in the passband, however, they exhibit not good enough stopband-rejection characteristics since only two inherent transmission zeros appear in the stopband. Whereas compact filters with higher selectivity and lower insertion loss are required in many applications, i.e., the diplexer and multiplexer, developing SIW dual-mode filters with miniature sizes and multiple transmission zeros is an efficient approach to suit these requirements.

In this paper, to generate more transmission zeros for achieving better frequency selectivity without enlarging sizes of the filter, a multilayer dual mode SIW filter using LTCC technology is investigated theoretically and experimentally. By introducing mixed coupling between source and load, the filter not only has four transmission zeros to improve frequency selectivity, but also has a small size by the virtue of its multilayer structure. An experimental filter configuration with central frequency of 10 GHz are fabricated and measured to validate the structure of the proposed model Design details are described, and both computed and experimental results are presented and discussed.

2. FILTER ANALYSIS AND DESIGN

2.1. Topology Diagram

The coupling schemes of a conventional extended doublet (ED) and a modified ED are show in Figures 1(a) and (b), where resonators 1 and 2 represent the two degenerated modes (TE_{102}/TE_{201}) in the first dual-mode resonator, and resonator 3 is formed using one of two degenerated modes in another dual-mode resonator, respectively. In other words, we only excite TE_{201} mode in the second dual-mode SIW resonator. Conventional topology of an ED filter without source-load coupling can obtain two transmission zeros in either side of the passband [33]. By adding source and load coupling into the ED, three transmission zeros can be generated. Under the circumstances, with introducing mixed coupling between the source and the load, i.e., mixed source and load coupling (MSLC), the fourth transmission zero can be obtained, which is shown in Figure 1(c). The coexistence of electric and magnetic coupling can be adopted to build dual-coupling paths between source and load to introduce additional transmission
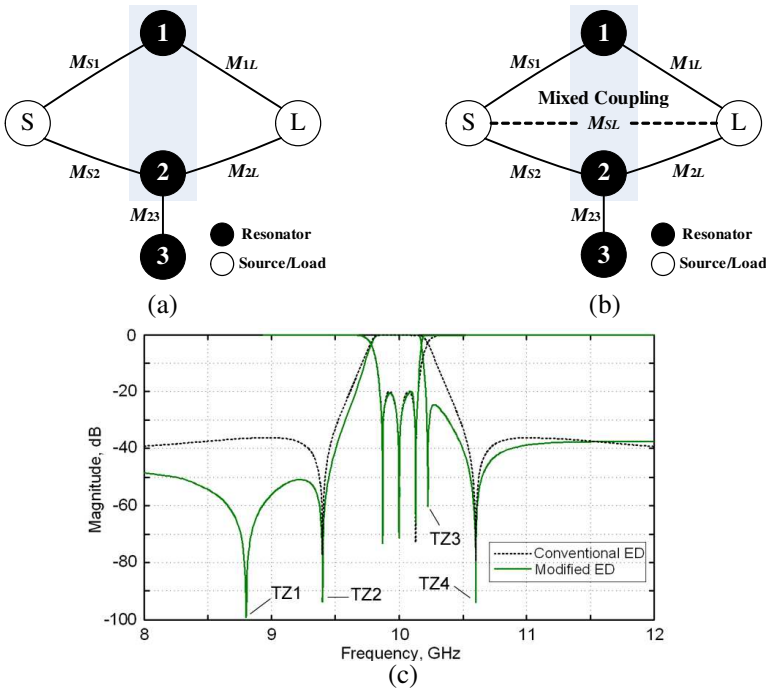
Figure 1. Coupling schemes and frequency response of the multilayer dual-mode filter. (a) Conventional extended doublet (ED) topology, (b) modified ED topology and (c) comparison of frequency response.

zero, which are usually controllable by adjusting the mixed coupling coefficients. That is to say, the source and the load are directly coupled which can add an additional transmission path based on conventional transversal doublet, and then mixed coupling between them can also bring another signal path to generate up to four transmission zeros [34]. The coupling matrix M of the proposed dual-mode SIW with modified ED topology can be written as

$$M = \begin{bmatrix} 0 & M_{S1} & M_{S2} & 0 & M_{SL}(\omega) \\ M_{S1} & M_{11} & 0 & 0 & M_{1L} \\ M_{S2} & 0 & M_{22} & M_{23} & M_{2L} \\ 0 & 0 & M_{23} & M_{33} & 0 \\ M_{SL}(\omega) & M_{1L} & M_{2L} & 0 & 0 \end{bmatrix} \quad (1)$$

where M_{S1}, M_{S2}, M_{1L} and M_{2L} represent the coupling between source/load and each resonator mode, respectively. M_{11}, M_{22} and M_{33} of diagonal elements in coupling matrix account for differences in the resonant frequencies of the resonators, and M_{23} express the coupling

between resonator 2 and 3. $M_{SL}(\omega)$ represents the mixed coupling between source and load.

The conventional ED filter has a pair of finite transmission zeros, and the governing equation of finite transmission zero can be expressed as [33]

$$\Omega^2 = \frac{M_{S1}^2 M_{23}^2}{M_{S1}^2 - M_{S2}^2} \tag{2}$$

When $|M_{S1}| < |M_{S2}|$, the pair of transmission zeros is on the imaginary-frequency axis. On the contrary, to generate a pair of real-frequency transmission zeros, it should be $|M_{S1}| > |M_{S2}|$. After introducing source-load coupling, an additional transmission path can be obtained in the modified ED, which can bring the third transmission zeros. To get more insight of location of three transmission zeros in this modified ED, an explicit expression relating the coupling elements and the transmission zero is given by

$$a\Omega^3 + b\Omega^2 + c\Omega + d = 0 \tag{3a}$$

Where

$$a = M_{SL}(\omega) \tag{3b}$$
$$b = (M_{11} + M_{22} + M_{33}) \cdot M_{SL}(\omega) + M_{S1}^2 - M_{S2}^2 \tag{3c}$$
$$c = \left(M_{11}M_{22} + M_{11}M_{33} + M_{22}M_{33} - M_{23}^2\right) \cdot M_{SL}(\omega)$$
$$+ (M_{22} + M_{33}) M_{S1}^2 - (M_{11} + M_{33}) M_{S2}^2 \tag{3d}$$
$$d = M_{11}\left(M_{22}M_{33} - M_{23}^2\right) \cdot M_{SL}(\omega)$$
$$+ \left(M_{22}M_{33} - M_{23}^2\right) M_{S1}^2 - M_{11}M_{33}M_{S2}^2 \tag{3e}$$

where $\Omega(\omega/\omega_0 - \omega_0/\omega)/FBW$ is normalized angular frequency while FBW is the fractional bandwidth. It is shown that three transmission zeros can be generated while introducing source-load coupling. Meanwhile, when source-load coupling becomes mixed coupling, i.e., MSLC, the coexistence of electric and magnetic coupling can be adopted to build dual-coupling paths between source and load to introduce the fourth transmission zero as shown in Figure 1(c).

2.2. Configuration of the Dual Mode Filter

To achieve flexible coupling manners with a more effective size reduction, a dual-mode SIW filter by embedding resonators into LTCC multilayer substrate is presented according to the coupling scheme in Figure 1(b). The overview of the proposed filter is illustrated in Figure 2. The filter consists of two resonant cavities, one input SIW and one output SIW. It should be noted that, compared to a
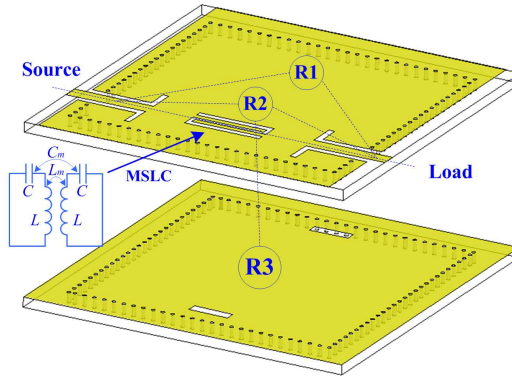
Figure 2. Three-dimensional view of the proposed dual mode filter with MSLC.

conventional cascade dual-mode SIW filter, two cavities of proposed filter are stacked vertically. Feeding structures with input/output current probes are offset from the center line of the SIW to excite the two resonant modes in the upper dual-mode cavity. Both TE_{102} and TE_{201} modes are two typically orthogonal degenerated resonant modes which are very similar to those in a conventional metal rectangular cavity. The coupling between the above and below resonant cavities could be realized though two rectangular slots in the middle of metal layer. Meanwhile, the coupling character as well as the coupling strength can be flexibly controlled by the position and the size of slots.

In addition, the interdigital slot-line (ISL) structure on the top metal layer is implemented to introduce mixed coupling between source and load [35]. $M_{SL}(\omega)$ in (3) represents the mixed coupling composed of electric and magnetic coupling between source and load. $M_{SL}(\omega)$ is related to frequency, which can be obtained by using the conventional solution method of a mixed coupling coefficient, as described in [34]

$$M_{SL}(\omega) = [\omega L_m - 1/(\omega C_m)]/\omega_0 L \tag{4}$$

where each resonator in the equivalent circuit of the two mixed coupled resonators is characterized by an inductance L together with a parallel capacitance C, as shown in Figure 2, and its resonant frequency equals to $\omega_0 = (LC)^{-1/2}$. L_m and C_m denote the coupling inductance and capacitance, and they will produce mixed magnetic and electric coupling, respectively. Moreover, the coupling coefficient at center frequency ω_0 is written as

$$k(\omega_0) = L_m(1 - \omega_m^2/\omega_0^2)/L \tag{5}$$

where $\omega_m = (L_m C_m)^{-1/2}$. Besides, it also has

$$M_{SL}(\omega) = k(\omega_0)\omega_0(\omega^2 - \omega_m^2)/[\omega(\omega_0^2 - \omega_m^2)] \tag{6}$$

Based on the equivalent network as shown in Figure 2, the coexistence of electric and magnetic coupling can be adopted to build dual-coupling paths between source and load, which could obtain additional transmission zero. The coupling mechanism for generating transmission zero is similar to that in [34]. Here, it can be noticed that mixed coupling coefficient is relative to frequency. It can be either positive or negative which can be considered separately for predigestion. When the mixed coupling coefficient is positive, namely, the infinite C_m inclines ω_m to 0. Then the coupling coefficient can be described as:

$$M_{SL}(\omega) = \omega L_m/\omega_0 L = \omega k(\omega_0)/\omega_0 \tag{7}$$

Meanwhile, when the coupling coefficient is negative, L_m inclines to 0, and ω_m inclines to infinite as a result. Then the coupling coefficient can be given as:

$$M_{SL}(\omega) = \omega_0 C/\omega C_m = \omega_0 k(\omega_0)/\omega \tag{8}$$

The proposed the topology can be implemented by the structure shown in Figure 3, and its normalized coupling coefficients using the gradient-based optimization method [36] are synthesized to be: $M_{S1} = 0.7856$, $M_{S2} = 0.5703$, $M_{1L} = -0.7856$, $M_{2L} = 0.5703$, $M_{23} = -1.156$, $M_{SL} = 0.2116$. Figures 4(a) and (b) show the E-field and H-field distributions of the proposed dual mode filter, respectively.
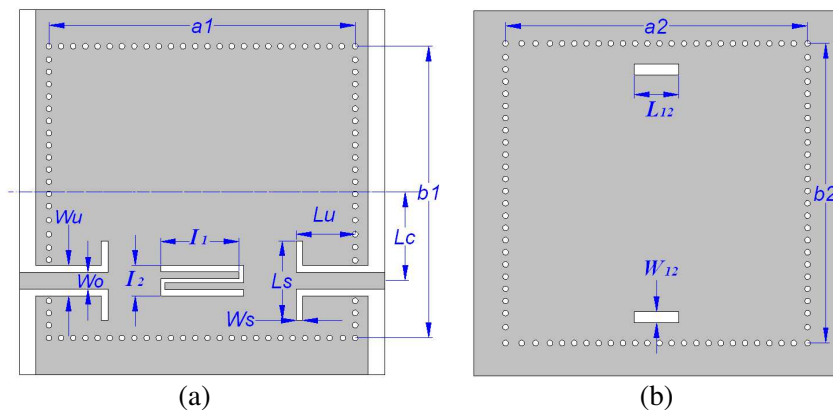
Figure 3. The configurations of proposed dual mode filter. (a) Top metal layer and (b) middle metal layer.
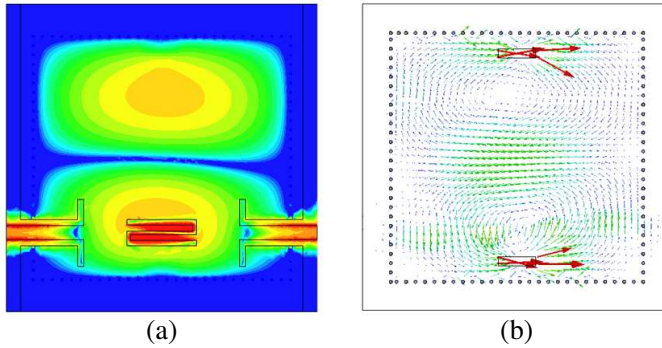
Figure 4. The E-field and H-field distributions of proposed dual mode filter: (a) E-field distributions of top metal layer and (b) H-field distributions of middle metal layer.

2.3. Locations of Transmission Zeros

As mention above, conventional ED without source-load coupling can obtain only two transmission zeros in its stopband. By introducing MSLC with frequency-variant coupling to ED, namely, modified ED as shown in Figure 1, two extra controllable transmission zeros will be generated in the stopband. Meanwhile, the levels of electric and magnetic coupling of MSLC which can tune the locations of transmission zeros are mainly controlled by the length (I_1) and the width (I_2) of ISL. Besides, the resonant frequency of the ISL is far from the central frequency of the filter, so the ISL almost does not affect the passband of the filter. The S_{21}-parameter of proposed SIW filter for different values of I_1 is shown in Figure 5(a). Transmission zeros TZ2 and TZ3 located at each side of its near passband are mainly dominated by previous ED structure, and TZ4 at upper stopband by source-load coupling. Hence locations of TZ2, TZ3 andTZ4 change slightly when varying the values of I_1. However, as an additional transmission zero caused by mixed coupling, TZ1 is much more sensitive to the values of I_1, i.e., TZ1 characterized by $\omega_m = (L_m C_m)^{-1/2}$ in the inset of Figure 2 will be produced by the mixed coupling between the source and load, and it has an obvious relationship with ω_0 as follows

$$\omega_0/\omega_m = (k_m/k_c)^{1/2} = (L_m C_m/LC)^{1/2} \tag{9}$$

where $k_m = L_m/L$ is the magnetic coupling part while $k_c = C/C_m$ is the electric coupling one. With increasing the values of I_1, i.e., adding coupling capacitance C_m, the electric coupling part ($k_c = C/C_m$) of the mixed coupling will become weaker. Under this circumstance, it

will result in the increment of ω_0/ω_m, as shown in Figure 5(a), and the additional transmission zero TZ1 at the far lower-stopband moves to lower frequencies.
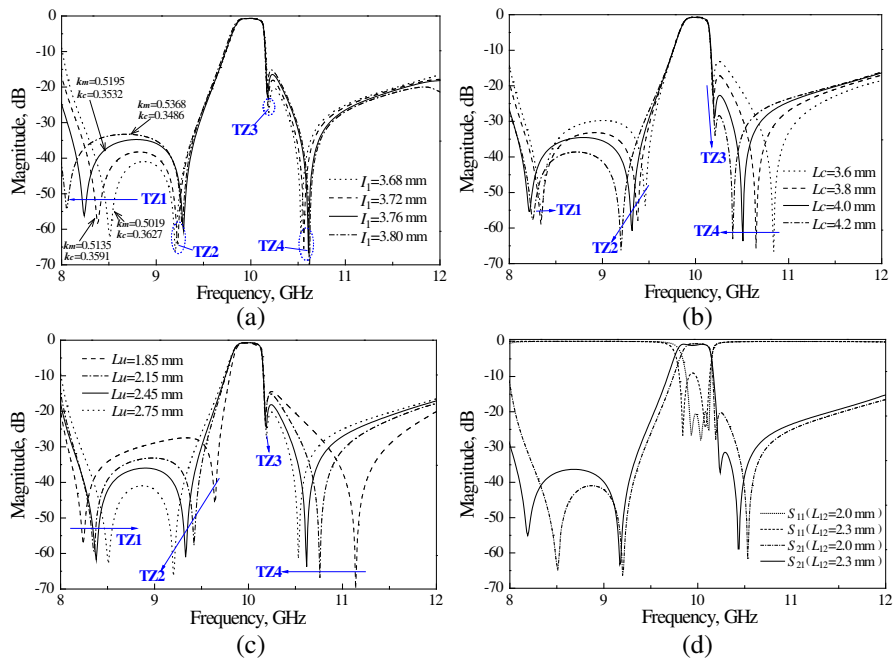
Figure 5. S-parameters for different values of (a) I_1, (b) L_c, (c) L_u and (d) L_{12}, respectively.

Figure 5(b) shows the S_{21}-parameter of the proposed filter for different values of L_c. As can be seen, the offset L_c between the center line and feeding structure of the dual-mode SIW filter also has obvious influence on the locations of the transmission zeros, other than TZ1. With increasing the values of L_c, TZ2 and TZ4 move towards the lower frequencies while TZ3 towards the opposite directions, whereas center frequency and bandwidth of the filter do not vary obviously. Meanwhile, the position of TZ1 at the far lower-stopband shifts slightly. Moreover, the sizes of input/output (I/O) current probes in feeding structure will have evident effect on the locations of transmission zeros and bandwidth of the filter. Figure 5(c) shows the S_{21}-parameter of the proposed filter with different values of lengths (L_u) of I/O current probes. It can be seen that the values of L_u affect locations of four transmission zeros obviously. With the values of L_u increase, TZ1 show a general tendency to move toward the center of passband, while on the

contrary TZ2 shifts away from the center of passband. Similarly, the locations of TZ3 and TZ4 show a common tendency to move together when increasing the length of L_u Furthermore, it should be noted that couplings between two multilayer cavities can also affect the bandwidth and in-band return loss of the filter. Figure 5(d) shows the S-parameter of the filter for different lengths of coupling slots (L_{12}) between two multilayer resonant cavities. In order to achieve demanded frequency responses during design process of the proposed dual-mode SIW filter, mixed couling structure and I/O current probes ought to be controlled and tuned together.

2.4. Multilayer Dual-mode Filter Design

To demonstrate the application of above-mentioned structure, a multilayer dual-mode SIW filter is implemented on an eight-layer substrate using LTCC material Ferro-A6 with relative dielectric constant of $\varepsilon_r = 5.9$, loss tangent of 0.0015. The filter is designed to have a central frequency of 10 GHz, a 3 dB fractional bandwidth of 3.0%, and four transmission zeros which are located at 8.5, 9.2, 10.2 and 10.5 GHz, respectively.

Every SIW unit is built on a four-layer substrate. The initial sizes of dual mode SIW resonator can be calculated by using the following equation

$$f_{res} = \frac{c}{2\pi\sqrt{\varepsilon_r}}\sqrt{\left(\frac{m}{L_{eff}}\right)^2 + \left(\frac{n}{W_{eff}}\right)^2} = \frac{c}{2\pi\sqrt{\varepsilon_r}}\sqrt{\left(\frac{p}{L_{eff}}\right)^2 + \left(\frac{q}{W_{eff}}\right)^2} \quad (10)$$

where m, n, p and q are indices of the mode, the only additional constrain of the dual-mode operation is that $m \neq p$ and $n \neq q$. In addition, for a square SIW cavity, its TE_{201} and TE_{102} modes resonate at the same frequency. c is the velocity of light in the vacuum, ε_r is the relative dielectric constant, L_{eff} and W_{eff} are the effective length and width of the resonant cavity given by

$$L_{eff} = l - \frac{d^2}{0.95p}, \quad W_{eff} = w - \frac{d^2}{0.95p}, \quad (11)$$

where l and w are the length and width of resonant cavity, respectively; d and p are the diameter of metallic via and the space between adjacent vias, respectively [11]. The complete filter parameters are fine tuned by slight alterations of each cavity resonator and each coupling in turn until the filter response is optimized to achieve the desired response by using commercial full wave electromagnetic simulation software HFSS.

Table 1. Parameters of the proposed filter (Unit: mm).

Symbol	$a1$	$b1$	L_c	L_{12}	L_s	L_u	I_1
Value	13.75	13.05	3.96	2.05	3.6	2.75	3.55
Symbol	$a2$	$b2$	W_o	W_{12}	W_s	W_u	I_2
Value	13.5	13.45	0.75	0.5	0.3	1.4	1.4
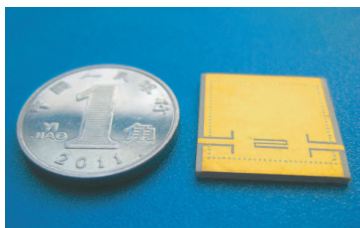
Figure 6. Photograph of fabricated filter.
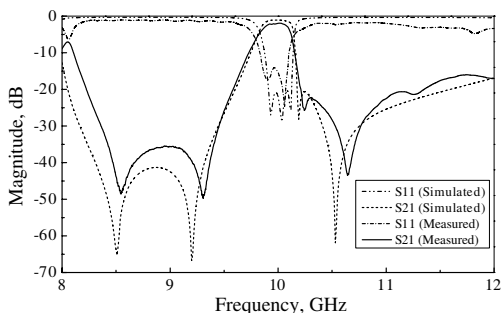
Figure 7. Measured and simulated frequency responses of the proposed filter.

3. EXPERIMENTAL RESULTS

The proposed multilayer dualmode SIW filter has been fabricated with LTCC process. The geometrical dimensions are summarized in Table 1. Figure 6 shows the photograph of the fabricated filter. By virtue of the multilayer structure and flexible mixed coupling manner, the overall size of the fabricated filter is only 16.4 mm × 16.4 mm × 0.8 mm. An Agilent E8363B vector network analyzer is used for measurement. The measured and simulated frequency responses are illustrated in Figure 7 which the measured results are in good agreement with the simulated ones. The measured central frequency is 10 GHz with a 3 dB fractional bandwidth of about 3.2% The spurious peak around 8 GHz is arose from the resonant frequency of ISL. The minimum passband insertion loss is about 1.93 dB, and in-band return loss is greater than 15.5 dB. Four transmission zeros are located at 8.55 GHz with 48.5 dB rejection, 9.32 GHz with 49 dB rejection, 10.25 GHz with 26 dB rejection, and 10.65 GHz with 43 dB rejection, respectively. The measured results are in good agreement with the simulated ones except a small frequency shift of transmission zeros and a little discrepancy in the in-band insertion loss. The frequency shift is mainly contributed to

the difference between the actual and nominal values of the dielectric constant. The degeneration of the in-band insertion loss are caused by the test fixture including SMA connectors and the manufacturing tolerance of LTCC process, such as conductor and dielectric loss, wrinkles of printing conductor surface and edge, and co-fireability of conductor and ceramic material. It should be noted that co-fireability between conductor and ceramic during the manufacturing process is main cause of the degeneration of the in-band insertion loss. If the material or process conditions of the ceramic and conductor are inappropriate, various macro and micro flaws may occur, which will worsen the in-band insertion loss. Furthermore, minute pores may be found forming at the interface in the co-firing process, which is yet another possible factor influencing the in-band insertion loss. To avoid these undesirable possibilities, it is not sufficient only to optimize the co-firing process condition or profile. Rather, it is also necessary in some cases to revise the base powder of each material in order to improve the co-fireability behavior of the conductor and ceramic. Overall, the proposed filter exhibits good frequency selectivity and compact size by profit from its modified ED and multilayer structure. Table 2 shows the comparison with some other recent works on dual-mode SIW filters. As can be seen, the proposed filter not only exhibits good selectivity owing to its modified ED with four controllable transmission zeros, but also has a compact size by profit from multilayer LTCC structure.

Table 2. Comparisons with some other dual-mode SIW filters.

Refs.	f_{center}	Min. Insertion Loss	BW	Nos. of TZs	Occupying Sizes
[28]	12 GHz	2.0 dB	11%	2	$35 \times 25 \, mm^2$
[32]	10 GHz	1.9 dB	3.3%	2	$> 30 \times 30 \, mm^2$
[27]	10 GHz	1.98 dB	5.5%	3	$27.5 \times 27.5 \, mm^2$
[37]	10 GHz	1.65 dB	3.4%	3	$> 32 \times 32 \, mm^2$
This work	10 GHz	1.93 dB	3.2%	4	$16.4 \times 16.4 \, mm^2$

4. CONCLUSION

Modified ED and its application to multilayer dual-mode SIW filter are presented. By implementing mixed coupling into the source and the load of the proposed structure, four transmission zeros are generated in the stopband to improve the frequency selectivity. An

experimental filter has been designed and fabricated using LTCC technology to validate the effectiveness of the proposed structure with good agreement obtained between their simulated and measured results. Furthermore, in virtue of flexible coupling manner of multilayer structure, the filters exhibit the merits of both miniature size and good selectivity. It is expected that the proposed filter will find applications in high-performance and high-integration microwave circuit design.

ACKNOWLEDGMENT

REFERENCES

1. Chaudhary, G., Y. Jeong, K. Kim, and D. Ahn, "Design of dual-band bandpass filters with controllable bandwidths using new mapping function," *Progress In Electromagnetics Research*, Vol. 124, 17–34, 2012.

2. Chiou, Y.-C. and J.-T. Kuo, "Planar multiband bandpass filter with multimode stepped-impedance resonators," *Progress In Electromagnetics Research*, Vol. 114, 129–144, 2011.

3. Kuo, J.-T., T.-W. Lin, and S.-J. Chung, "New compact triple-mode resonator filter with embedded inductive and capacitive cross coupling," *Progress In Electromagnetics Research*, Vol. 135, 435–449, 2013.

4. Wong, S. W., K. Wang, Z. N. Chen, and Q. X. Chu, "Rotationally symmetric coupled-lines bandpass filter with two transmission zeros," *Progress In Electromagnetics Research*, Vol. 135, 641–656, 2013.

5. Gao, M.-J., L.-S. Wu, and J.-F. Mao, "Compact notched ultra-wideband bandpass filter with improved out-of-band performance using quasi electromagnetic bandgap structure," *Progress In Electromagnetics Research*, Vol. 125, 137–150, 2012.

6. Lee, K., T.-H. Lee, Y.-S. Kim, and J. Lee, "New negative coupling structure for substrate-integrated cavity resonators and its application to design of an elliptic response filter," *Progress In Electromagnetics Research*, Vol. 137, 117–127, 2013.

7. Chen, C.-H., C.-S. Shih, T.-S. Horng, and S.-M. Wu, "Very miniature dual-band and dual-mode bandpass filter designs on an integrated passive device chip," *Progress In Electromagnetics Research*, Vol. 119, 461–476, 2011.

8. Wei, C.-L., B.-F. Jia, Z.-J. Zhu, and M.-C. Tang, "Design of different selectivity dual-Mode filters with E-shaped resonator," *Progress In Electromagnetics Research*, Vol. 116, 517–532, 2011.

9. Xia, B. and J. Mao, "A dual mode filter with wideband suppression," *Journal of Electromagnetic Waves and Applications*, Vol. 26, Nos. 11–12, 1470–1475, 2012.

10. Park, W.-Y. and S. Lim, "Bandwidth tunable and compact band-pass filter (BPF) using complementary split ring resonators (CSRRS) on substrate integrated waveguide (SIW)," *Journal of Electromagnetic Waves and Applications*, Vol. 24, Nos. 17–18, 2407–2417, 2010.

11. Chen, X. P., K. Wu, and D. Drolet, "Substrate integrated waveguide filter with improved stopband performance for satellite ground terminal," *IEEE Trans. Microw. Theory Tech.*, Vol. 57, No. 3, 674–683, 2009.

12. Jiang, W., W. Shen, L. Zhou, and W.-Y. Yin, "Miniaturized and high-selectivity substrate integrated waveguide (SIW) bandpass filter loaded by complementary split-ring resonators (CSRRs)," *Journal of Electromagnetic Waves and Applications*, Vol. 26, Nos. 11–12, 1448–1459, 2012.

13. Chen, X. P. and K. Wu, "Substrate integrated waveguide cross-coupled filter with negative coupling structure," *IEEE Trans. Microw. Theory Tech.*, Vol. 56, No. 1, 142–149, 2008.

14. Jedrzejewski, A., N. Leszczynska, L. Szydlowski, and M. Mrozowski, "Zero-pole approach to computer aided design of in-line SIW filters with transmission zeros," *Progress In Electromagnetics Research*, Vol. 131, 517–533, 2012.

15. Chen, Y. J., "Substrate integrated waveguide frequency-agile slot antenna and its multibeam application," *Progress In Electromagnetics Research*, Vol. 130, 153–168, 2012.

16. Shen, W., W.-Y. Yin, X.-W. Sun, and J.-F. Mao, "Compact coplanar waveguide-incorporated substrate integrated waveguide (SIW) filter," *Journal of Electromagnetic Waves and Applications*, Vol. 24, No. 7, 871–879, 2010.

17. Zhang, Q.-L., W.-Y. Yin, S. He, and L.-S. Wu, "Evanescent-mode substrate integrated waveguide (SIW) filters implemented with complementary split ring resonators," *Progress In Electromagnetics Research*, Vol. 111, 419–432, 2011.

18. Shen, W., W. Y. Yin, and X. W. Sun, "Miniaturized dual-Band substrate integrated waveguide filter with controllable bandwidths," *IEEE Microw. Wireless Compon. Lett.*, Vol. 21, No. 8, 418–420, 2011.

19. Zhang, Q. L., B. Z. Wang, W. Y. Yin, and L. S. Wu, "Design of a miniaturized dual-band double-folded substrate integrated waveguide bandpass filter with controllable bandwidths," *Progress In Electromagnetics Research*, Vol. 136, 211–223, 2013.

20. Huang, Y. M., Z. H. Shao, and L. F. Liu, "A substrate integrated waveguide bandpass filter using novel defected ground structure shape," *Progress In Electromagnetics Research*, Vol. 135, 201–213, 2013.

21. Wu, L. S., X. L. Zhou, W. Y. Yin, L. Zhou, and J. F. Mao, "A substrate-integrated evanescent-mode waveguide filter with nonresonating node in low-temperature co-fired ceramic," *IEEE Trans. Microw. Theory Tech.*, Vol. 58, No. 10, 2654–2662, 2010.

22. Xu, Z. Q., Y. Shi, B. C. Yang, P. Wang, and Z. Tian, "Compact second-order LTCC substrate integrated waveguide filter with two transmission zeros," *Journal of Electromagnetic Waves and Applications*, Vol. 26, Nos. 5–6, 795–805, 2012.

23. Wu, L. S., X. L. Zhou, Q. F. Wei, and W. Y. Yin, "An extended doublet substrate integrated waveguide (SIW) bandpass filter with a complementary split ring resonator (CSRR)," *IEEE Microw. Wireless Compon. Lett.*, Vol. 19, No. 12, 777–779, 2009.

24. Wu, L.-S., J.-F. Mao, W. Shen, and W.-Y. Yin, "Extended doublet bandpass filters implemented with microstrip resonator and full-/half-mode substrate integrated cavities," *Progress In Electromagnetics Research*, Vol. 101, 203–216, 2010.

25. Li, R. Q., X. H. Tang, and F. Xiao, "An novel substrate integrated waveguide square cavity dual-mode filter," *Journal of Electromagnetic Waves and Applications*, Vol. 23, Nos. 17–18, 2523–2529, 2009.

26. Shen, W., X. W. Sun, W. Y. Yin, J. F. Mao, and Q. F. Wei, "A novel single-cavity dual mode substrate integrated waveguide filter with non-resonating node," *IEEE Microw. Wireless Compon. Lett.*, Vol. 19, No. 6, 368–370, 2009.

27. Xu, Z. Q., Y. Shi, C. Y. Xu, and P. Wang, " A novel dual mode substrate integrated waveguide filter with mixed source-load coupling (MSLC)," *Progress In Electromagnetics Research*, Vol. 136, 595–606, 2013.

28. Qin, P.-Y., C.-H. Liang, B. Wu, and T. Su, "Novel dual-mode bandpass filter with transmission zeros using substrate

integrated waveguide cavity," *Journal of Electromagnetic Waves and Applications*, Vol. 22, Nos. 5–6, 723–730, 2008.

29. Lee, J. H., S. Pinel, J. Laskar, and M. M. Tentzeris, "Design and development of advanced cavity-based dual-mode filters using low-temperature co-fired ceramic technology for V-band gigabit wireless systems," *IEEE Trans. Microw. Theory Tech.*, Vol. 55, No. 9, 1869–1878, 2007.

30. Wei, Q. F., Z. F. Li, and H. G. Shen, "Dual-mode filters based on substrate integrated waveguide by multilayer LTCC technology," *Microw. Opt. Tech. Lett.*, Vol. 50, No. 11, 2788–2790, 2008.

31. Ahn, K. and I. Yom, "A Ka-band multilayer LTCC 4-pole bandpass filter using dual-mode cavity resonators," *2008 IEEE MTT-S International Microwave Symposium Digest*, 1235–1238, Jun. 2008.

32. Zhang, Z. G., Y. Fan, Y. J. Cheng, and Y. H. Zhang, "A compact multilayer dual-mode substrate integrated circular cavity (Sicc) filter for X-band application," *Progress In Electromagnetics Research*, Vol. 122, 453–465, 2012.

33. Liao, C.-K., P.-L. Chi, and C.-Y. Chang, "Microstrip realization of generalized Chebyshev filters with box-like coupling schemes," *IEEE Trans. Microw. Theory Tech.*, Vol. 55, No. 1, 147–153, 2007.

34. Chu, Q. X. and H. Wang, "A compact open-loop filter with mixed electric and magnetic coupling," *IEEE Trans. Microw. Theory Tech.*, Vol. 56, No. 2, 431–439, 2008.

35. Shen, W., Wu, L. S., Sun, X. W., Yin, W. Y, and J. F. Mao, "Novel substrate integrated waveguide filters with cross coupling (MCC)," *IEEE Microw. Wireless Comp. Lett.*, Vol. 19, No. 11, 701–703, 2009.

36. Amari, S. and U. Rosenberg, "New building blocks for modular design of elliptic and self-equalized filters," *IEEE Trans. Microw. Theory Tech.*, Vol. 52, No. 2, 721–736, 2004.

37. Zhang, Z. G., Y. Fan, Y. J. Cheng, and Y. H. Zhang, "A novel multilayer dual-mode substrate integrated waveguide complementary filter with circular and elliptic cavities (SICC and SIEC)," *Progress In Electromagnetics Research*, Vol. 127, 173–188, 2012.